THIN FILMS

Giant polarization in super-tetragonal thin films through interphase strain

Linxing Zhang[1], Jun Chen[1,2]*, Longlong Fan[1], Oswaldo Diéguez[3], Jiangli Cao[4], Zhao Pan[1], Yilin Wang[1], Jinguo Wang[5], Moon Kim[5], Shiqing Deng[6], Jiaou Wang[7], Huanhua Wang[7], Jinxia Deng[1], Ranbo Yu[1], James F. Scott[8], Xianran Xing[1,2]*

Strain engineering has emerged as a powerful tool to enhance the performance of known functional materials. Here we demonstrate a general and practical method to obtain super-tetragonality and giant polarization using interphase strain. We use this method to create an out-of-plane–to–in-plane lattice parameter ratio of 1.238 in epitaxial composite thin films of tetragonal lead titanate ($PbTiO_3$), compared to 1.065 in bulk. These thin films with super-tetragonal structure possess a giant remanent polarization, 236.3 microcoulombs per square centimeter, which is almost twice the value of known ferroelectrics. The super-tetragonal phase is stable up to 725°C, compared to the bulk transition temperature of 490°C. The interphase-strain approach could enhance the physical properties of other functional materials.

Controlling strain can enhance the properties of multifunctional materials, such as magnetoresistance, superconductivity, ferroelectricity, and antiferromagnetism (*1*–*4*). Among strained ferroelectrics (*5*–*8*), perovskite oxides with giant tetragonality (c/a) have a large value of polarization and a high Curie temperature (T_C) as a consequence of their large dipolar moment (*4*, *9*–*12*). However, these compounds are rare and generally require extreme synthesis conditions. One example of such an approach is applying high compressive pressure with diamond anvil cells (*11*, *12*), such as for $PbVO_3$ and $BiCoO_3$. Another approach, based on using a particular biaxial strain imposed by lattice-mismatched substrates on films, has been successfully applied in many cases (*1*, *10*, *13*, *14*). It is also possible to use isotropic strain to affect the structure and properties of materials (*11*, *12*, *15*–*18*). In particular, it has been shown that isotropic tensile strain (negative pressure) theoretically increases tetragonality and polarization of perovskite oxides, such as $BaTiO_3$ and $PbTiO_3$ (fig. S1) (*15*). Experimentally, negative pressure in $PbTiO_3$ nanowires was achieved by taking advantage of the phase transformation–induced stress, resulting in enhanced physical properties (*17*, *18*). However, engineering such high negative pressure in experiments is challenging; a simpler practical approach is therefore desired, especially for epitaxial films.

Here we investigate such a concept, termed "interphase strain." To introduce a large strain, two materials with similar crystal structures, but different lattice parameters, are grown in a single epitaxial composite such that, on the boundaries between them, their lattice parameters are matched. This is different from the conventional composite, in which different phases have their own lattice parameters. In this way, an isotropic tensile or compression strain can be introduced into the material that originally had the smaller or larger lattice parameters, respectively; we call this interphase strain. Here the concept of interphase strain has been implemented to induce a negative pressure in $PbTiO_3$ epitaxial composite ferroelectric thin films via PbO. This results in the enhancement of the polarization and out-of-plane–to–in-plane lattice parameter (c/a) ratio and the highest stable temperature (T_{stable}) of the super-tetragonal phase in the $PbTiO_3$ film.

The epitaxial composite films were grown on $SrTiO_3$ (STO) substrates by using a simple radio-frequency magnetron sputtering. The atomic deposition rate can be controlled by the oxygen ratio of the deposition environment, as discussed below. The samples of $PbTiO_3$ composite films were prepared without oxygen and with 9% oxygen, referenced as PT (I) and PT (II), respectively. If either of the PT (I) or PT (II) samples is annealed above 725°C, then a new atomic structure is obtained, classified as PT (III). Figure 1A highlights a small region (17° to 24°) of the general x-ray diffraction (XRD) patterns, demonstrating the apparent change in the c lattice parameters of PT (I), PT (II), and PT (III). In these and the results of high-resolution XRD patterns covering a large angle region (15° to 75°) (fig. S2A), only diffraction peaks from the directions of (100) STO substrate and (001) films can be observed. This suggests that all films are epitaxial growth. Additional phi scans of both (101) and (103) planes of PT (I), which were measured along the corresponding lattice plane of the substrate, feature a four-axis symmetric structure, confirming an in-plane epitaxial relationship with the substrate (Fig. 1C).

The typical epitaxial $PbTiO_3$ films [PT (III)] reveal the normal c lattice parameter of ~4.08 Å that is established in the literature (*19*). By contrast, the primitive PT (II) and PT (I) grown on the same STO substrate exhibit strong reflections at anomalous values corresponding to the c lattice parameters of ~4.408 and ~4.840 Å, respectively. Subsequent synchrotron-based x-ray reciprocal space mappings (RSMs) about the (103) plane of the films and substrates (Fig. 1B) verify that the a lattice parameter is well matched between the substrates and the films, but the c lattice parameters of the films are very different from that of the bulk. The position of the c lattice parameter of bulk $PbTiO_3$, which is similar to that of the normal coherently strained $PbTiO_3$ thin films [PT (III)], is indicated by the dashed line for comparison. Notably, increases in the c lattice parameter by 16.5 and 6.1%, as compared to the bulk value (*20*), are observed in PT (I) and PT (II), respectively. Furthermore, both c and c/a increase with increasing thickness of PT (I) or PT (II) (Fig. 1, D and E, and table S1), which indicates that the growth strain is weakly controlled by the substrate, as discussed in table S1.

$PbTiO_3$ has a tetragonal perovskite structure with lattice parameters a = 3.899 Å, c = 4.154 Å, and c/a = 1.065 (Fig. 2A) (*20*). The precursor PbO, which is used to prepare $PbTiO_3$, has a similar tetragonal structure, although derived from the fluorite structure, but with a large c/a ratio (a = 3.9729 Å, c = 5.0217 Å, and c/a = 1.264) (Fig. 2B) (*21*). The perovskite-like periodic configuration can be identified in the plate-like PbO, as indicated by the red rectangle in Fig. 2B. The similarity in structure between the $PbTiO_3$ and PbO configurations offers the potential for realizing the heteroepitaxial growth with interphase strain. Experimentally, to obtain such self-assembled heteroepitaxial composite films of the stretched $PbTiO_3$ with the compressed PbO, the atomic deposition rate was controlled effectively for their different growth kinetics. The Pb-rich composition determined by chemical analysis (inductively coupled plasma optical emission spectrometry) is uniform throughout the films detected by Auger electron spectroscopy with depth analysis (Fig. 2C), except for the higher Pb concentration on the surface. This verifies the homogeneous and randomly alternate growth of $PbTiO_3$ and PbO in both PT (I) and PT (II) (fig. S3). The dashed circles in Fig. 2D highlight different lattice configurations and contrast them with their surroundings. The fast Fourier transform (FFT) pattern taken from a typical example of the regions marked by the dashed circles features a tetragonal structure but with an extinction of (100) plane. It reveals that these regions are PbO (Fig. 2F). However, the other surrounding regions

[1]Department of Physical Chemistry, University of Science and Technology Beijing, Beijing 100083, China. [2]State Key Laboratory for Advanced Metals and Materials, University of Science and Technology Beijing, Beijing 100083, China. [3]Department of Materials Science and Engineering, Faculty of Engineering, The Raymond and Beverly Sackler Center for Computational Molecular and Materials Science, Tel Aviv University, Tel Aviv 6997801, Israel. [4]Institute of Advanced Materials and Technology, University of Science and Technology Beijing, Beijing 100083, China. [5]Department of Materials Science and Engineering, University of Texas at Dallas, Richardson, TX 75080, USA. [6]National Center for Electron Microscopy in Beijing, School of Materials Science and Engineering, The State Key Laboratory of New Ceramics and Fine Processing, Key Laboratory of Advanced Materials (MOE), Tsinghua University, Beijing 100084, China. [7]Institute of High Energy Physics, Chinese Academy of Sciences, Beijing 100049, China. [8]School of Chemistry and School of Physics, St Andrews University, St Andrews, Fife KY16 9ST, Scotland.
***Corresponding author. Email: junchen@ustb.edu.cn (J.C.); xing@ustb.edu.cn (X.X.)**

provide a typical FFT pattern for the super-tetragonal $PbTiO_3$ structure (Fig. 2E). The results indicate that the metastable PbO is randomly distributed in $PbTiO_3$. The direct evidence for the heteroepitaxial structure between $PbTiO_3$ and PbO in the present PT (I) is provided by the spherical aberration–corrected high-angle annular dark-field (HAADF) *Z*-contrast scanning transmission electron microscope (STEM) image (Fig. 2G). The bright, light gray, and dark gray contrast spots correspond to Pb ($Z = 82$, where Z is the atomic number), Sr ($Z = 38$), and Ti ($Z = 22$) columns, respectively, owing to the Z^2-dependent contrast (*6*, *22*). The intensity profile along the red dashed line in Fig. 2H reveals a transition from Ti of $PbTiO_3$ to Pb of PbO, indicating a good lattice matching at the $PbTiO_3$/PbO interface (Fig. 2I). Both $PbTiO_3$ and PbO in PT (I) have the same *c* lattice parameter (4.840 Å) (Figs. 1 and 2G). Hence, in the present PT (I) epitaxial thin films, PbO suffers a small out-of-plane compression strain of 3.6%, whereas a giant tensile strain (16.5%) exists in $PbTiO_3$ (Fig. 1B). The defect dipoles generated in such special environments usually cannot produce such giant strains (*16*).

Investigations with HAADF-STEM ($c/a = 1.224$) (Fig. 2) underpin the giant c/a ratio of $PbTiO_3$ in PT (I) ($c/a = 1.226$-1.238, table S1), as determined from both macroscopic XRD and synchrotron-based RSMs about the (103) plane (Fig. 1). This c/a value is much larger than that of bulk (1.065) or in any other previously reported results for $PbTiO_3$ (*17*). It is comparable to the c/a value of the super-tetragonal phases that appear in the biaxial-strained $BiFeO_3$ films (1.232) and in those perovskite-type compounds synthesized by high-pressure and high-temperature methods, such as $PbVO_3$ (1.229), and $BiCoO_3$ (1.267) (*10*–*12*).

Intriguingly, the c/a ratio can be adjusted by controlling the oxygen ratio during the growth of thin films. For example, the sample PT (II) was prepared with 9% oxygen, which features not only a smaller c/a (1.142) but also a lower Pb concentration than that of PT (I) (Fig. 1, table S2, and figs. S3 and S4). Therefore, the oxygen ratio affects the Pb atomic deposition rate of the $PbTiO_3$ epitaxial composite thin films. To grow the present super-tetragonal films, an atmosphere with deficient oxygen is required for fast PbO nucleation. The volume fractions of $PbTiO_3$ are 100, 80, and 45.3% for the PT (III), PT (II), and PT (I) thin films, respectively. The amount of PbO in the present films determines the c/a ratio, which further reveals the role of PbO in interphase strain. Unlike studies that introduce biaxial strain, the present method of interphase strain has little dependence on substrates. Super-tetragonal films such as PT (I) can also be successfully obtained on other lattice-mismatched substrates, such as inexpensive $LaAlO_3$ or sapphire, indicating that the super-tetragonality is not caused by substrate biaxial strain stemming from either Poisson or electrostriction effects (see detailed discussion in table S1 and figs. S5 and S6).

To further characterize the interface between $PbTiO_3$ and PbO, we carried out first-principles calculations. To model this system of PT (I), the volume fraction of $PbTiO_3$ was set as 50%, which is comparable to that of 45.3% in PT (I). Hence, we used a number of infinitely extended layers of $PbTiO_3$ matched to an equal number of infinitely extended layers of PbO for four possible sets of planes: (100), (110), (101), and (001). For the (100) case, we did this for groups that included 3, 5, and 7 layers containing Pb; for the (110) and (101) cases, 6 and 10 layers (Fig. 3A); and for the (001) case, 3 and 5 layers. In all cases, the atomic configurations were fully relaxed until the forces between atoms were below 0.01 eV/Å and the stresses on the cell were below 0.01 GPa. As depicted in Fig. 3B, the calculations of c/a ratio, lattice parameters, and displacement of the Ti atom (δz_{Ti}) with respect to the center of the cage of surrounding Pb atoms converged well with increasing numbers of layers. For the (100), (110), and (101) interfaces, the c/a ratio is around 1.22, in excellent agreement with the experimental result for PT (I); even for the (001) interface, c/a is almost 1.2.

A giant c/a ratio is normally associated with a large polarization in perovskite oxides. The polarization hysteresis loops feature a remanent polarization (P_r) of PT (I) as large as 236.3 μC/cm^2 (Fig. 4A and fig. S7). Intriguingly, the present polarization of PT (I) is higher than for other ferroelectrics (Fig. 4B) (*10*, *23*–*25*). For example, it is 1.8 times as large as that of the tetragonal-like $BiFeO_3$ epitaxial thin films (130 μC/cm^2) and 3.4 times as large as that of the strained $BaTiO_3$ thin films (70 μC/cm^2) (*10*, *25*). It is also much larger than the calculated values for the spontaneous polarization of Pb- or Bi-based perovskites with large c/a ratios, such as $PbVO_3$ (179 μC/cm^2) and $BiCoO_3$ (152 μC/cm^2) (*26*). The nature of the giant polarization can also be directly revealed by the large δz_{Ti}, as displayed in fig. S6 (*17*, *27*). In PT (I), the STEM result for the δz_{Ti} value is 0.474 Å, almost three times as large as that for bulk $PbTiO_3$ (0.162 Å) (*28*), which directly reveals the crystal-lattice origin of the giant spontaneous polarization. Furthermore, the δz_{Ti} value of first-principles calculations is comparable to the one found experimentally (Fig. 3B). Hence, there is likely a strong electrostatic interaction at the phase boundary of the ferroelectric-paraelectric interfaces between $PbTiO_3$ and PbO (*29*), resulting in the strong polarization. In the PT (II) thin films, a relatively large P_r (129.6 μC/cm^2) was also observed (fig. S8). P_r and c/a are correlated linearly (inset of Fig. 4A). The local stability of the ferroelectric switching supported by piezoelectric measurements of piezoresponse force microscopy still needs to be further confirmed (figs. S8 and S9).

PbO contributes little to the polarization (figs. S10 to S13), the PT (I) thin films show negligible leakage current (fig. S14), and the giant polarization

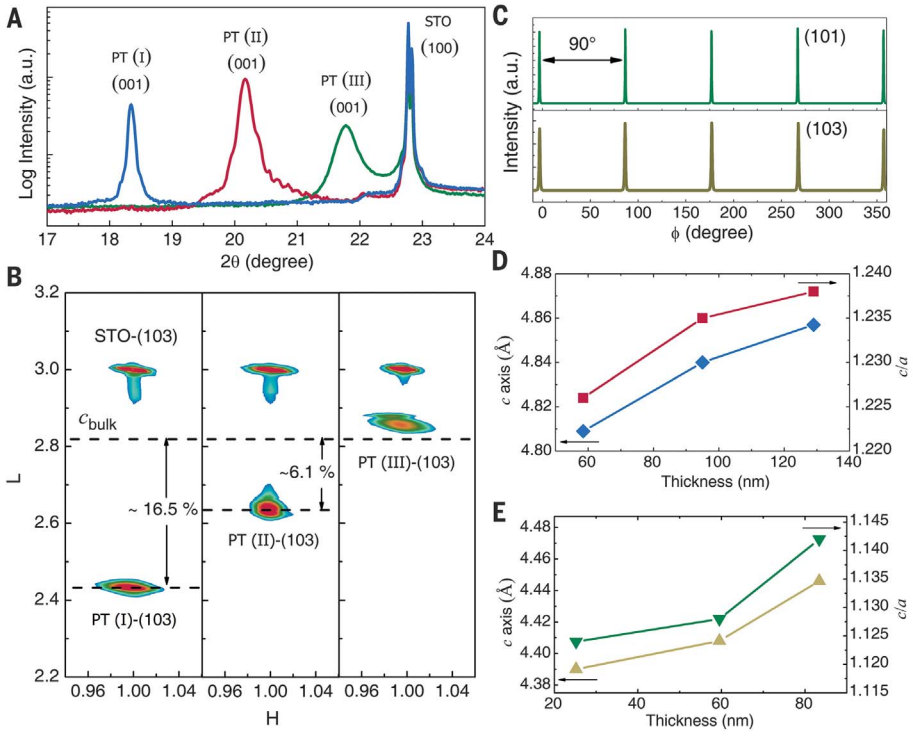

Fig. 1. Crystal structure characterization of epitaxial composite films. (**A**) Out-of-plane XRD of (001) peaks of PT (I), PT (II), and PT (III) epitaxial thin films on (100) STO substrates. a.u., arbitrary units. (**B**) Synchrotron-based (103) x-ray RSM study of PT (I), PT (II), and PT (III) epitaxial thin films about the STO (103) diffraction condition. L, crystal index of (00l); H, crystal index of (h00). (**C**) The phi scans of both (101) and (103) planes of PT (I), demonstrating a four-axis symmetric structure. ϕ, the angle at which the sample rotates around its normal line. (**D** and **E**) The lattice parameters of *c* and c/a of (D) PT (I) and (E) PT (II) as a function of film thickness. The data are tabulated in table S1.

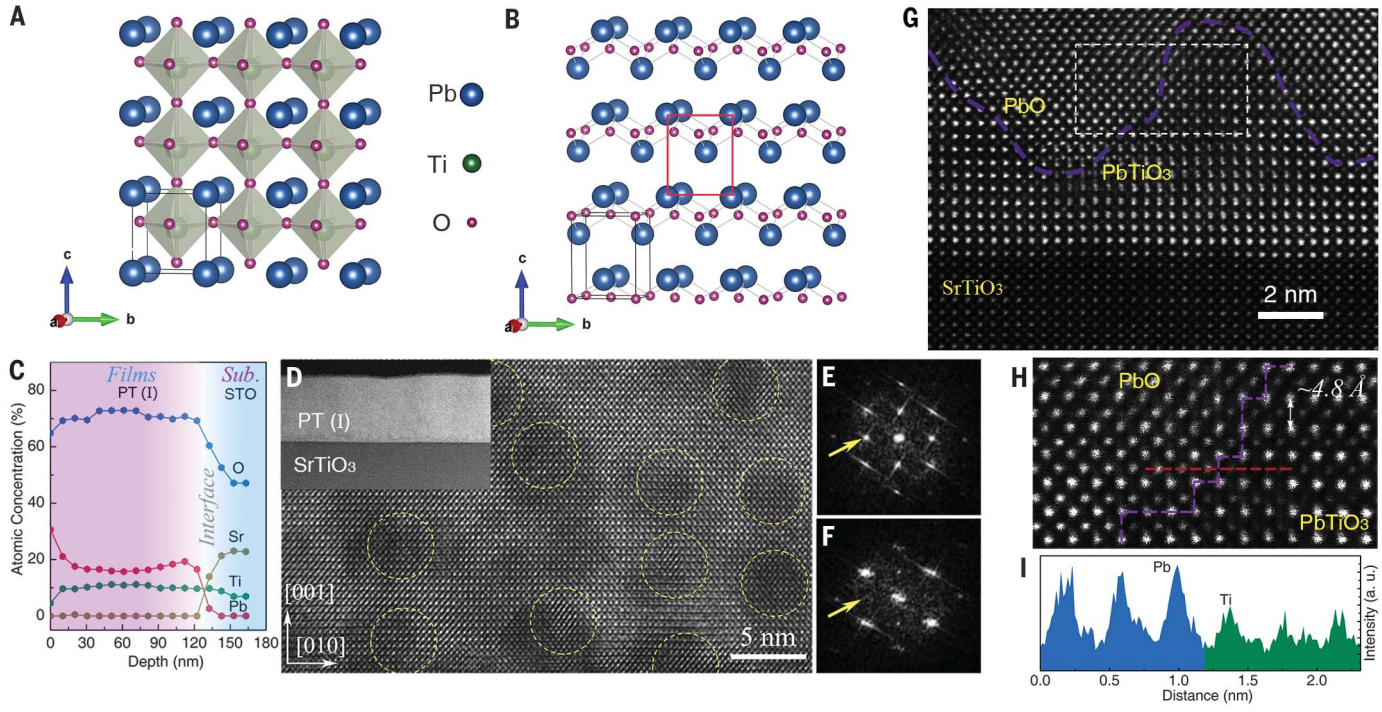

Fig. 2. Atomic-resolution microstructure of epitaxial composite films. (**A**) Crystalline structure of $PbTiO_3$. (**B**) Crystalline structure of PbO. The red rectangle indicates the perovskite-like periodic configuration. (**C**) Atomic-concentration depth analysis by Auger electron spectroscopy of the PT (I) thin films. Sub., substrate. (**D**) High-resolution transmission electron microscopy image along the *a* axis of the PT (I) thin films. The inset displays a low-magnification cross-sectional image. The regions indicated by the yellow dashed circles represent PbO. (**E**) The FFT pattern taken from the regions surrounding the yellow dashed circles of (D), featuring the $PbTiO_3$ structure. The yellow arrow indicates the (100) plane of $PbTiO_3$. (**F**) The FFT pattern taken from a typical example of the regions marked by yellow dashed circles of (D), featuring the PbO structure. The yellow arrow indicates the extinction of the (100) plane of PbO. (**G**) HAADF-STEM image of the heteroepitaxial interface between $PbTiO_3$ and PbO, as viewed along the *a* axis of the PT (I) thin film. The purple dashed line shows the approximate interface of $PbTiO_3$/PbO. The detailed discussion of the interface between film and substrate is in fig. S6. (**H**) Enlarged view of the region enclosed by the white rectangle in (G), verifying that $PbTiO_3$ and PbO have the same lattice parameters. (**I**) Intensity profile along the red dashed line in (H), directly revealing the transition from Ti to Pb. a.u., arbitrary units.

phenomenon has been observed in many samples (fig. S7). The slanted "lozenge-shaped" hysteresis loop would imply incomplete saturation (fig. S7E). The optimization of the loops is not just a matter of increased voltage; for such a large polarization, the switching can be current limited by the rise time of the switching pulse, as first determined for lead zirconate titanate (*30*), and the switching frequency should also be optimized. Some hysteresis loops exhibited several discrete steps (fig. S18), suggesting that the slanted loop in Fig. 4A is related to the continuous multilevel switching in these composites of ferroelectric $PbTiO_3$ and dielectric PbO. Similar multistep polarization processes can arise from the switching of superdomain blocks and were first observed in $Pb(Zr_{0.2}Ti_{0.8})O_3$ (PZT) (*31*). The switching effect is related to the ferroelastic-ferroelectric coupling. The observation of a multistep polarization process and the stable shape of the hysteresis loop, as a function of temperature or frequency, lend evidence to support that the present thin film is intrinsically ferroelectric (see detailed discussions in the supplementary text and figs. S15 to S18).

Temperature-dependent XRD was performed to determine the super-tetragonal phase stability of the present films. As depicted in Fig. 4C, the T_{stable} of the super-tetragonal phase of PT (I) is up to 725°C, compared with the T_C (490°C) of bulk $PbTiO_3$ (*20*). PT (I) exhibits the highest temperature for ferroelectric phase in all reported $PbTiO_3$ studies. According to the Landau-Ginzburg-Devonshire theory or Abrahams-Kurtz-Jamieson relationship for perovskite oxides (*17*, *27*), if the super-tetragonal structure of PT(I) was more stable against temperature, the ferroelectric-to-paraelectric phase transition (~1000°C) would be even higher. The cyclic curves reveal a stable super-tetragonal structure for PT (I) if temperatures are increased to 650°C (fig. S19B). In the tetragonal phase, the *c* lattice parameter of PT (I) features a positive thermal expansion similar to that of PbO, which indicates that PbO determines the thermal expansion of $PbTiO_3$ (table S3). However, at temperatures higher than 725°C, an irreversible structural collapse occurs because of the PbO extraction and volatility (table S2), in which the *c* lattice parameter collapses from the large value of 4.92 Å in the PT (I) to the normal value of 3.98 Å in the PT (III). At the same time, the excess PbO is isolated from the lattice of $PbTiO_3$ as a second phase (fig. S20). A huge volume contraction (19%) occurs at the structure-collapse temperature in PT (I).

To further elucidate the mechanism of the giant polarization in PT (I), we have studied its electronic hybridization using x-ray absorption spectroscopy (XAS) (fig. S21). On the basis of crystal-field theory, the fivefold-degenerated 3d level splits into doublet e_g and triplet t_{2g} levels in the octahedral symmetry (*32*) (fig. S21A). The weakened splitting of e_g in PT (I) with enhanced *c*/*a* indicates larger Ti^{4+} distortion (off-center displacement) (fig. S21C). The linear relation between the energy difference between the peaks in the L_3 e_g level (ΔE) and *c*/*a* is similar to that between δz_{Ti} and *c*/*a*, resulting in the linear relation between polarization and *c*/*a* shown in the inset of Fig. 4A. This further verifies the giant polarization of PT (I). Furthermore, both the decrease in the energy difference between the two main peaks of the L_3 or L_2 edges and the lower intensity of L_3 t_{2g} or L_2 t_{2g} indicate the enhanced ionic distortion and the existence of Ti^{3+} ions in the PT (I) thin films. This is in good agreement with the O K-edge XAS and XPS (figs. S22 and S23). The existence of Ti^{3+} ions would cause additional imperfections in the crystal with increasing distortions and also enhance the polarization (fig. S23).

We conclude by emphasizing the complete internal consistency of the data presented here: the large saturation and remanent polarizations, the STEM- and XAS-measured displacement of

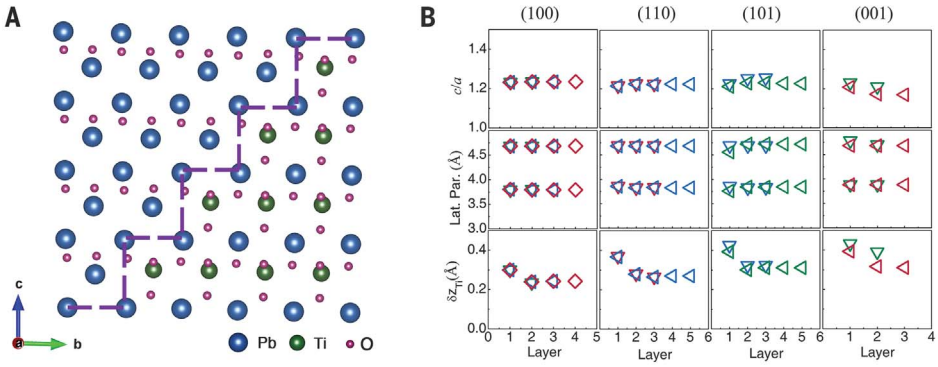

Fig. 3. Calculations of $PbTiO_3$/PbO interfaces. (**A**) Example of the $PbTiO_3$/PbO system in our calculations (periodic boundary conditions apply): $PbTiO_3$/PbO (101) interface (purple dashed line), as viewed along the *a* axis. (**B**) Structural results of density functional theory calculations of four different $PbTiO_3$/PbO interfaces. Top row: tetragonal *c*/*a* ratio; middle row: *c* and *a* lattice parameters; bottom row: displacement of Ti atom. Layer, the unit cell layer of $PbTiO_3$ starting at the interface of $PbTiO_3$/PbO.

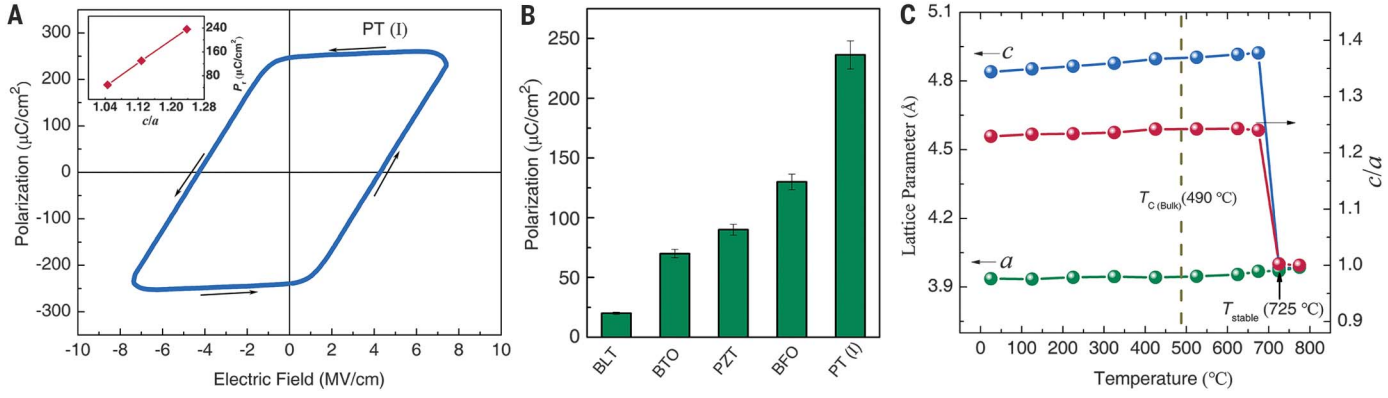

Fig. 4. Properties of the PT (I) epitaxial composite films. (**A**) Polarization versus electric field hysteresis loop of the PT (I) thin films with a thickness of 129 nm grown on 0.7 weight % Nb-doped STO with Pt top electrode. The inset depicts the remanent polarization as a function of *c*/*a*. The arrows indicate the counterclockwise direction of testing time in the hysteresis loop. (**B**) Comparison of polarization of the present PT (I) thin films with the previously experimentally measured P_r in films, from left to right: $Bi_{3.25}La_{0.75}Ti_3O_{12}$ (BLT) (*23*), strained $BaTiO_3$ (BTO) (*24*), unstrained $Pb(Zr_{0.2}Ti_{0.8})O_3$ (PZT) (*25*), and strained $BiFeO_3$ (BFO) (*10*). (**C**) Temperature dependence of lattice parameters and *c*/*a* of PT (I). The position of T_C of bulk $PbTiO_3$ is indicated by the dotted line for comparison.

the Ti atom, and the high T_{stable} of the super-tetragonal phase. We also stress some advantages of the present method, which could create a distinct pathway for material design: (i) The interphase strain can provide not only isotropic tensile strain but also isotropic compressive strain, (ii) the level of strain can be modulated by adjusting the composition (fig. S24), and (iii) the generation of strain in thin films can be independent from the choice of substrates.

REFERENCES AND NOTES

1. D. G. Schlom *et al.*, *MRS Bull.* **39**, 118–130 (2014).
2. J.-P. Locquet *et al.*, *Nature* **394**, 453–456 (1998).
3. R. von Helmolt, J. Wecker, B. Holzapfel, L. Schultz, K. Samwer, *Phys. Rev. Lett.* **71**, 2331–2333 (1993).
4. H. Béa *et al.*, *Phys. Rev. Lett.* **102**, 217603 (2009).
5. A. K. Yadav *et al.*, *Nature* **530**, 198–201 (2016).
6. Y. L. Tang *et al.*, *Science* **348**, 547–551 (2015).
7. P. Zubko *et al.*, *Nature* **534**, 524–528 (2016).
8. D. Lee *et al.*, *Science* **349**, 1314–1317 (2015).
9. R. J. Zeches *et al.*, *Science* **326**, 977–980 (2009).
10. J. X. Zhang *et al.*, *Phys. Rev. Lett.* **107**, 147602 (2011).
11. A. A. Belik, M. Azuma, T. Saito, Y. Shimakawa, M. Takano, *Chem. Mater.* **17**, 269–273 (2005).
12. A. A. Belik *et al.*, *Chem. Mater.* **18**, 798–803 (2006).
13. J. Wang *et al.*, *Science* **299**, 1719–1722 (2003).
14. J. H. Lee *et al.*, *Nature* **466**, 954–958 (2010).
15. S. Tinte, K. M. Rabe, D. Vanderbilt, *Phys. Rev. B* **68**, 144105 (2003).
16. A. R. Damodaran, E. Breckenfeld, Z. Chen, S. Lee, L. W. Martin, *Adv. Mater.* **26**, 6341–6347 (2014).
17. J. Wang *et al.*, *Nat. Mater.* **14**, 985–990 (2015).
18. A. Kvasov *et al.*, *Nat. Commun.* **7**, 12136 (2016).
19. C. Lichtensteiger, J. M. Triscone, J. Junquera, P. Ghosez, *Phys. Rev. Lett.* **94**, 047603 (2005).
20. S. A. Mabud, A. M. Glazer, *J. Appl. Cryst.* **12**, 49–53 (1979).
21. H. E. Swanson, R. K. Fuyat, *Natl. Bur. Stand. (US) Circular* **539**, 30–33 (1953).
22. G. Catalan *et al.*, *Nat. Mater.* **10**, 963–967 (2011).
23. B. H. Park *et al.*, *Nature* **401**, 682–684 (1999).
24. K. J. Choi *et al.*, *Science* **306**, 1005–1009 (2004).
25. V. Nagarajan *et al.*, *J. Appl. Phys.* **86**, 595–602 (1999).
26. Y. Uratani, T. Shishidou, F. Ishii, T. Oguchi, *Jpn. J. Appl. Phys.* **44**, 7130–7133 (2005).
27. S. C. Abrahams, S. K. Kurtz, P. B. Jamieson, *Phys. Rev.* **172**, 551–553 (1968).
28. A. M. Glazer, S. A. Mabud, *Acta Crystallogr. B* **34**, 1065–1070 (1978).
29. E. Khestanova *et al.*, *Adv. Funct. Mater.* **26**, 6446–6453 (2016).
30. P. Larsen, G. Kampschöer, M. B. van der Mark, M. Klee, in *ISAF'92: Proceedings of the Eighth Institute of Electrical and Electronics Engineers (IEEE) International Symposium on Applications of Ferroelectrics (ISAF)* (IEEE, 1992), pp. 217–224.
31. P. Gao *et al.*, *Nat. Commun.* **4**, 2791 (2013).
32. K.-T. Ko *et al.*, *Nat. Commun.* **2**, 567 (2011).

ACKNOWLEDGMENTS

We thank Q. Liu, P. Hang, and Y. Cai for the preparation of electrodes by photolithography at the University of Science and Technology Beijing; Q. Wang and Z. Che for the preparation of STEM samples by focused ion beam at the University of Texas at Dallas; and D. Zheng for the analysis of piezoresponse force microscopy at Tianjin University. We are grateful for the use of the Beijing Synchrotron Radiation Facility (1W1A and 4B9B beamlines, China) and the Shanghai Synchrotron Radiation Facility (BL14B1 beamline, China) of the Chinese Academy of Sciences. **Funding:** This work was supported by the National Natural Science Foundation of China (grant nos. 91422301, 21731001, and 21590793), the Changjiang Young Scholars Award, the National Program for Support of Top-Notch Young Professionals, and the Fundamental Research Funds for the Central Universities, China (grant nos. FRF-TP-17-001B and FRF-TP-17-030A1). O.D. acknowledges funding from the Israel Science Foundation through grant nos. 1814/14 and 2143/14. **Author contributions:** J.Ch., L.Z., and X.X. conceived the idea of the work. L.Z., J.Ca., L.F., Z.P., Y.W., R.Y., and J.D. fabricated the films and performed the initial tests. O.D. performed the theoretical calculations. Jin.W., M.K., and S.D. performed and analyzed the STEM experiments. Jia.W. conducted the synchrotron x-ray absorption spectroscopy measurements. H.W. conducted the synchrotron x-ray diffraction characterizations. J.F.S. analyzed and discussed the data of ferroelectric properties. L.Z. and J.Ch. wrote the manuscript with contributions from others. All authors discussed the results and commented on the manuscript. J.Ch. and X.X. guided the projects. **Competing interests:** The authors declare no competing interests. **Data and materials availability:** All data are presented in the main text and supplementary materials.

SUPPLEMENTARY MATERIALS

www.sciencemag.org/content/361/6401/494/suppl/DC1
Materials and Methods
Supplementary Text
Figs. S1 to S24
Tables S1 to S3
References (*33*–*56*)
Data S1

17 March 2017; accepted 31 May 2018
10.1126/science.aan2433

Giant polarization in super-tetragonal thin films through interphase strain

Linxing Zhang, Jun Chen, Longlong Fan, Oswaldo Diéguez, Jiangli Cao, Zhao Pan, Yilin Wang, Jinguo Wang, Moon Kim, Shiqing Deng, Jiaou Wang, Huanhua Wang, Jinxia Deng, Ranbo Yu, James F. Scott and Xianran Xing

Science **361** (6401), 494-497.
DOI: 10.1126/science.aan2433

An epitaxial route to strain

Strain can have a dramatic effect on the properties of materials. Zhang *et al.* introduced a large strain in the material $PbTiO_3$ by growing it epitaxially in a composite with PbO. On the boundaries between the two materials, their normally different lattice constants were matched, giving rise to the strain. As a consequence, the films exhibited a very large electric polarization even in the absence of an electric field. The method may be applicable to generating other functional materials.

Scence, this issue p. 494